# Fabrication of Electrostatically Actuated MEMS Switch

Mattias Herrfurth, Department of Microelectronic Engineering, *Rochester Institute of Technology*

***Abstract* —** This paper summarizes the process of designing, fabricating, and analyzing a series of MEMS switches. These devices are composed of a mechanical conductive polysilicon material being brought into contact to a signal line so as to rectify it. The parameters altered between each switch include the number of arms anchoring the mechanical polysilicon to the substrate and various dimensional constants. These dimensional constants include values for the width and length of the arms, and the area of the electrodes used in the electrostatic operation. Two sets of devices were fabricated for this paper, and data was obtained for the advancement of the MEMS fabrication process. A new design rule was formulated for this process, and device layout considerations were made to optimize the design for making a DC contact switch.

***Index Terms* — MEMS – microelectromechanical systems; electrostatic actuation – the practice of applying opposing charges to materials in proximity of one another to cause them to attract**

## I. Introduction

There are several applications that MEMS devices have in modern and future electronics. It is desirable to find interesting and exploitable properties of MEMS devices for these applications. There are several sources of literature outlining the desirable properties of MEMS switches in comparison to traditional MOSFET and BJT based electronic architectures [2]. The properties of MEMS being investigated in particular, with respect to traditional architectures, are parameters of the insertion loss, electrical isolation, and power consumption. Published research and experiments have determined that these properties are found to be optimized in MEMS switches compared to MOSFETs [1][2].

This makes sense because the switch does not need to utilize the semiconductor properties of silicon and related crystalline materials. Therefore, there is very little source of electrical leakage in MEMS switches, so the isolation can be said to be notably high. Furthermore, since the incorporation of low-doped semiconductor materials is not necessarily required, it is possible to implant high levels of dopants and increase the conductivity of the device. Optimally, the only notable resistance to be seen in the circuit is that of the contact resistance between the mechanical polysilicon and the open circuit nodes. Additionally, this allows the power dissipation to be low, since the resistance is low. Ideally, there is no leakage current associated with a MEMS switch, since the "channel" in which switching occurs is physically an open circuit when the device is off. With no leakage current, the device can have even lower power consumption.

These properties allow for the application to many different fields of electronics, but in particular there is the interest of using these devices with electronics that are powered by scavenged energy. Scavenged energy devices refer to devices that produce electrical bias or current by absorbing and transforming a different type of energy into electrical energy. Examples of these types of devices include piezoelectrics, photovoltaics, thermoelectrics, etc. The energy obtained from these types of devices is typically very low compared to traditional sources of energy. Therefore, the circuits dependent on these sources will require very low power consumption to operate. MEMS devices have the potential for very low power consumption, so would be ideal for these applications. Scavenging energy, also known as energy harvesting, itself also has several applications, and one of particular note is that which will apply to electronics associated with the "Internet of Things", which is the movement towards electronics being integrated into many items and objects used in culture and day-to-day life. These applications do not require incredibly small transistors and logical gates, since most items in day-to-day life are macro-sized by many orders of magnitude compared to semiconductor industry standards. Therefore, devices in the internet of things could incorporate MEMS based logical operations very handily, since current MEMS devices require more space than traditional MOSFET devices.

The following figures illustrate the operation of a one-armed electrostatically actuated MEMS switch:

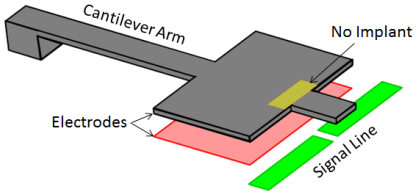


**Figure 1 - Single-arm MEMS switch (open)**

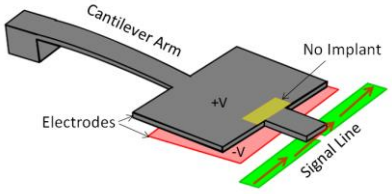


**Figure 2 - Single-arm MEMS switch (closed)**

The device pictured in figure 1 is a simplified representation of the type switch to be fabricated for this project in the open, off-state position, whereas the device in figure 2 is in the closed, on-state position. This device operates through the use of electrostatic force being applied using a voltage bias on an electrode of material beneath a cantilever of flexible and conductive material, which is also biased with an opposing voltage to that of the substrate electrode. When these two materials are biased in opposition to each other (i.e. -5V on the substrate electrode; +5V on the cantilever electrode), an electrostatic force occurs between the materials, pulling them together. This allows the signal line to be rectified, and able to transmit information.

This study is particularly interested in analyzing the effect that different dimensional parameters have on the fabrication and operation of MEMS switches. There is a separate investigation included in this study into the digital logic operation of these devices, which involves the design and fabrication of several types of basic logic gates.

## II. Theory

In order to design the MEMS switch utilizing electrostatic actuation, it is required to understand the forces involved in such operation. Three key equations were used to calculate the force required for the cantilever to make contact and the amount of voltage needed to cause this electrostatic actuation. These equations are as follows [3]:

$$F_{1-arm} = \frac{Y_{max} 3Ebh^3}{12L^3} \quad (1)$$

$$F_{2-arm} = \frac{Y_{max} 4Ebh^3}{L^3} \quad (2)$$

$$F_{emf} = \frac{\varepsilon_0 \varepsilon_r A V^2}{2d^2} \quad (3)$$

Where $F_{1arm}$ is the force required to deflect a one-armed cantilever, $F_{2arm}$ is the force required to deflect a two-armed cantilever, and $F_{emf}$ is the electrostatic force produced from some level of voltage across the electrodes $V$. In equations 1 and 2, $Y_{max}$ is the maximum deflection required for the cantilever to make contact to the signal line, $E$ is Young's Modulus, $b$ is the lateral arm width, $h$ is the vertical thickness of the arm, $L$ is the length of the arm. For a one-armed device, this L is measured from the anchor to the end of the arm, and for the two- and four-armed devices, L is measured from anchor to anchor along the meanders. In equation 3, $\varepsilon_o$ *and* $\varepsilon_r$ are the permittivity of free space and the relative permittivity of the polysilicon, respectively, $A$ is the area of the electrodes used for electrostatic actuation, $V$ is the voltage across the electrodes, and $d$ is the vertical distance between the electrodes. It should be noted that release holes in the mechanical polysilicon exist to allow the sacrificial oxide to be etched away at the last step of processing. These holes were taken into consideration in calculations for the electrostatic force, such that the total area of the electrode was multiplied by a factor of 0.84 to represent the amount of area subtracted by the holes.

The parameters that were altered between designs in this study include the area of actuating electrodes, the arm width, and arm length of each type of design, as well as the number of meanders in the four-arm device. The one- and two-armed MEMS switches are original designs to this paper. The four-armed MEMS switch was based off of the design created by Artur Nigmatulin as part of his Master's Thesis [4]. From his design, several parameters were changed in the same fashion as the one and two-armed MEMS switch. The following images represent the designs for each of the three switches.

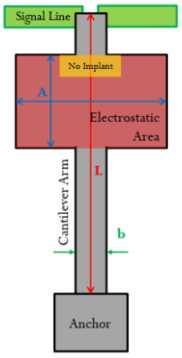


**Figure 3 - Design for one-armed MEMS switch**

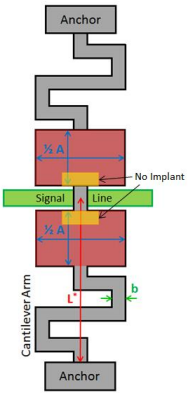


**Figure 4 - Design for two-armed MEMS switch**

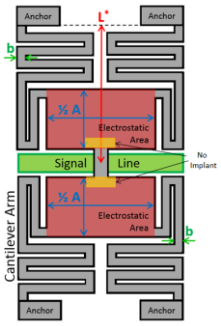


**Figure 5 - Design for four-armed MEMS switch**

In these figures, the gray material is the mechanical polysilicon, anchored at different points depending on the device type. The green signal line is open beneath the polysilicon overlapping it, and the yellow rectangles represent where the ion implant for the mechanical polysilicon is masked. The length of each device is represented by $L$ or $L^*$, where $L^*$ is not the value used in eq. (2), but is rather used to more easily represent the difference in device dimensions. As can be seen

in figure 4 and 5, the total electrostatic area *A* is the sum of the opposing electrode areas, and the arm width *b* is measured as shown.

Equations 1-3 were used in order to predict the operation of several different designs of MEMS switches. In total, 18 designs of the one- and two-armed MEMS switches were made, while 16 designs were made for the four-armed switch. A separate design of logic gates using smaller MEMS switches was also created as a proof of concept for the digital logic applications of these devices. The following tables summarize the full factorial design of experiment for this set of different device designs.

| One Arm Parameters | | | |
|---|---|---|---|
| L [μm] | 240 | 290 | N/A |
| b [μm] | 6 | 10 | 20 |
| A [$\mu m^2$] | 2000 | 5000 | 8000 |

**Table 1 - Design parameters for one-armed MEMS switch**

| Two Arm Parameters | | | |
|---|---|---|---|
| L* [μm] | 280 | 340 | N/A |
| b [μm] | 4 | 6 | 8 |
| A [$\mu m^2$] | 6600 | 7700 | 9300 |

**Table 2 - Design parameters for two-armed MEMS switch**

| Four Arm Parameters | | |
|---|---|---|
| L* [μm] | 300 | 320 |
| b [μm] | 5 | 7 |
| A [$\mu m^2$] | 212000 | 22600 |
| M [#] | 3 | 4 |

**Table 3 - Design parameters for four-armed MEMS switch**

A full factorial of these parameters was created, and the tables for the full experiment can be seen in the appendix tables A1-A3. For the design of the one- and two-armed MEMS switches, three values were used for both the area of the electrodes and the arm width, whereas only two values were used for the arm length. Given the complexity of the four-armed design, only two values were used for all three parameters, and a parameter for the number of meanders was added.

The MEMS switch operates using electrical bias applied across the electrostatic electrodes. Since the substrate polysilicon cannot move, this causes the cantilever to be pulled towards the substrate. The electrodes themselves have a coating of an insulating material, isolating them from each other in the case they come into contact. The mechanical polysilicon itself is brought into contact or proximity of an open circuit, and this contacting portion of the arm is electrically isolated from the rest of the arm, which has a bias applied. This arm coming into contact/proximity with the open circuit allows for a signal to be sent through the circuit, whereas no signal could be sent if the circuit remained open. This is how a relay operates. It should be noted that depending on whether the cantilever is brought into contact or into proximity with the open circuit will determine what type of signal can be sent through. With the cantilever in contact, a DC or AC signal can be sent through. If the cantilever is brought only within proximity with the open circuit, then an AC signal can be sent through, since the proximity will simulate two capacitors in series.

## III. Fabrication Process

For this paper, two sets of devices were designed for fabrication. The first set began fabrication in Fall 2015 as part of the MCEE-770 MEMS Fabrication course, and was designed to be a proof-of-concept for building these devices using the current process flow in development. The second set began fabrication in Spring 2016 and was designed as an experiment into investigating the effect that different device dimensions would have on the fabrication and operation of these switches. The fabrication process used for these devices is still in development and was first proposed in the summer of 2014 [5].

A total of eight mask levels are utilized in this process flow [5]. These steps include patterns for an interconnect polysilicon, anchor etch, sacrificial oxide, implant masking, mechanical polysilicon, contact cut etch, aluminum metal, and a release etch of the sacrificial oxide. A separate step for etching global alignment marks is also performed before any other patterning is done to the wafer. In total, the process involves approximately 50 processing steps, with breaks in processing to test for electrical conductivity of different deposited layers so as to confirm etching and patterning processes.

The following is a simplified version of the process flow for the fabrication of these devices:

*1)* ***Zero level alignment marks:*** Etch alignment marks into the substrate at the edge of the wafer
*2)* ***Interconnect polysilicon:*** Deposit, implant, and etch the substrate interconnecting polysilicon; passivate
***3) Anchor etch:*** Etch openings in passivation on interconnect polysilicon
***4) Sacrificial oxide:*** Deposit TEOS oxide and etch
***5) Implant masking:*** Deposit mechanical polysilicon and block implant in key areas; passivate
***6) Mechanical polysilicon:*** Etch patterns and release holes into mechanical polysilicon
***7) Contact cut:*** Etch openings in passivation for metal contacts
***8) Aluminum metal:*** Deposit and etch aluminum
***9) Release:*** Etch away sacrificial oxide; "release" mechanical polysilicon

## IV. Testing Procedure

In order to confirm that the devices fabricated perform the way they are expected to, it is required to develop a procedure to electrically test them under a variety of conditions. As can be seen in figures 2 and 3, there are four electrical connections that need to be made to the device in order to have it operate. These connections include voltage bias connections for the electrodes

(V+ and V-) and an input and output connection (VIN/$V_{in}$ and VOUT/$V_{out}$). These devices were designed to be tested using a 12 probe card installed on an HP4145.

The process for testing these devices will depend on the condition that either direct contact or proximity contact be made between the mechanical and substrate polysilicon layers. As previously stated, if direct contact can be made, then either a DC or an AC signal can be sent from input to output. If only proximity occurs between the two polysilicon layers, then only an AC signal can be sent through, since this proximity will act as two capacitors in series in the signal line.

In record the voltage bias required to pull the mechanical polysilicon close enough to the substrate to turn the switch on, it will be required to sweep a voltage across the electrodes and apply a signal to the input while measuring the response in the output. This procedure will be used for all the designs of the switches. As for the logic gates, they will be tested by sending logical voltage biases in and measuring the outputs to see if they represent the logical operation required of them.

## V. Results and Analysis

Both sets of devices, as of the time of the writing of this paper, are still in fabrication. The first set of devices has been fabricated up to the release level, which happens to be the most difficult step of the process. Release is when the sacrificial oxide is etched away, leaving the mechanical polysilicon suspended above the substrate. The operation of this step is very delicate and critical to obtaining a functional device. The second set of devices has been fabricated up to the metal level, which has encountered an unknown issue related to etching the metal. The following images are of the devices at the last successfully performed processing step.

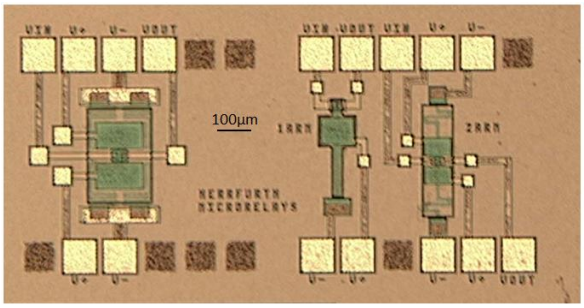


**Figure 6 - First set of devices (pre-release level)**

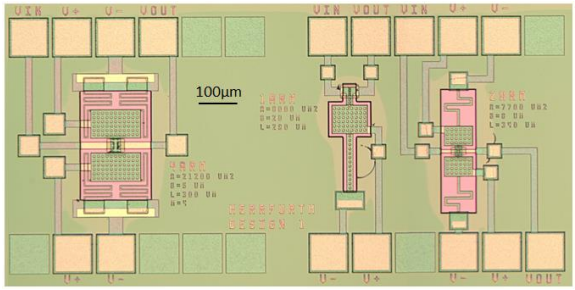


**Figure 7 - Second set of devices (Design 1; pre-metal)**

As can be seen from figures 6 and 7, these devices were designed to be tested using a 12-probe card. The devices of figure 6 have had metal deposited and etched, whereas the devices of figure 7 have had contact cut etches done in preparation of metal deposition.

A few issues arose during the processing of the second set of devices. These include an improperly processed anchor level photolithography which caused an incomplete etching of the interconnect polysilicon passivation in some locations on the wafers. Weeks were spent trying to recover this error. In addition to this, it was found that a design error had occurred which required the mask for the mechanical polysilicon to be reordered. However, from this error, a new design rule was created. It states that where an anchor cut is performed over the interconnect polysilicon, there must be either sacrificial oxide or mechanical polysilicon covering this area. Otherwise, the exposed interconnect polysilicon will be etched during the etching of the mechanical polysilicon. The following figure illustrates the correction made to the design based on these findings:

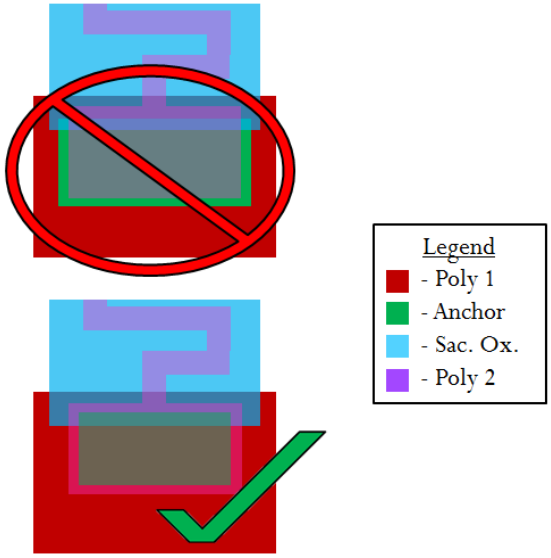


**Figure 8 - Implementation of the new design rule**

As can be seen in figure 8, the top design has an anchor layer on the interconnect polysilicon that is not covered by sacrificial oxide or mechanical polysilicon. Therefore, the uncovered interconnect polysilicon in this region will likely be etched when the mechanical polysilicon etch occurs.

As previously stated, the second set of devices has reached the metal level. Aluminum was deposited via evaporation, whereas the original process flow calls for a sputter deposition. It was assumed that these depositions would yield the same results, but it has been observed that aluminum is not being completely etched away in small features on the devices. It is unclear at this time as to why this etch is unsuccessful, but it may require a plasma etch instead of a wet etch to be completed.

It should be stated that the fabrication of the second set of devices was the first time fabrication was attempted by parties other than Dr. Lynn Fuller and Adam Wardas. As a result, more data and perspective on this process was acquired so that the MEMS fabrication process can be developed into a more robust flow. As a specific example, the photolithography process for etching the mechanical polysilicon is very sensitive, since it is required to etch relatively small holes into the polysilicon to be used in the release etch, and the topology at this step is

incredibly varied. This varying topology affects the exposure in relation to how much depth of focus is possible by the stepper system. In the processing of the first set of devices, many experiments were performed by Dr. Fuller and Adam Wardas to optimize these parameters, which were then tested by the second set of devices fabricated.

Another result of taking into consideration how these devices would be fabricated was how specifically a DC contact switch could be made. In order to make DC contact between the mechanical and interconnect polysilicon, it was determined that an anchor level cut be made into the interconnect polysilicon before the sacrificial oxide be deposited. This allows both for the interconnect polysilicon to be exposed underneath the mechanical polysilicon after the release layer. It also causes a physical depression in the mechanical polysilicon over the signal line since the anchor cut removes a significant thickness of nitride and oxide, allowing the mechanical polysilicon at this site to be significantly lower than the polysilicon above the passivated interconnecting polysilicon. This depression would theoretically allow for the mechanical polysilicon to be better able to contact the interconnect polysilicon.

## VI. Conclusion

From this study, several designs for electrostatically actuated MEMS switches were created. Considerations were made as to how these switches would best be fabricated using the current surface MEMS fabrication process. More perspective and data was collected in order to aid in the developing and refining process of creating a robust fabrication flow. While the two sets of devices did not complete fabrication, it is possible that once the release and metal layer processes for these devices is more fully understood, these devices will complete fabrication.

## VII. References


[1] H. Kam, "Design, Optimization, and Scaling of MEM Relays for Ultra-Low-Power Digital Logic," IEEE Trans. Electron Devices, vol. 58, no. 1, pp. 236-250, Jan., 2011

[2] T. K. Liu. (2012). *MEMS Switch for Low-Power Logic* [Online]. http://spectrum.ieee.org/semiconductors/devices/mems-switches-for-low-power-logic

[3] L. Fuller. (2015). *MEMS Mechanical Fundamaentals* [Online]. Available FTP: people.rit.edu Directory: lffeee/ File: MEMS_Mechanical_Fundamentals.pdf

[4] A. Nigmatulin. "DC-Contact MEMS Switch for Wireless Communication." M.S. thesis, Rochester Institute of Technology, USA, 2011.

[5] L. Fuller, A. Wardas. (2016). *Surface MEMS Fabrication Details* [Online]. Available FTP: people.rit.edu Directory: lffeee/ File:SurfaceMEMsFabricationDetails.pdf


## VIII. Appendix

| Design | Area (A) (um^2) | Arm width (b) (um) | Arm Length (L) (um) |
|---|---|---|---|
| 1 | 8000 | 20 | 290 |
| 2 | 2000 | 20 | 290 |
| 3 | 8000 | 10 | 290 |
| 4 | 2000 | 10 | 290 |
| 5 | 8000 | 20 | 240 |
| 6 | 2000 | 20 | 240 |
| 7 | 8000 | 10 | 240 |
| 8 | 2000 | 10 | 240 |
| 9 | 5000 | 10 | 290 |
| 10 | 5000 | 10 | 240 |
| 11 | 5000 | 20 | 290 |
| 12 | 5000 | 20 | 240 |
| 13 | 8000 | 6 | 240 |
| 14 | 8000 | 6 | 290 |
| 15 | 5000 | 6 | 240 |
| 16 | 5000 | 6 | 290 |
| 17 | 2000 | 6 | 240 |
| 18 | 2000 | 6 | 290 |

**Table A1 - Full factorial design for one-armed MEMS switch**

| Design | Area (A) (um^2) | Arm width (b) (um) | Arm length (L) (um) |
|---|---|---|---|
| 1 | 7700 | 8 | 340 |
| 2 | 7700 | 6 | 340 |
| 3 | 6600 | 8 | 340 |
| 4 | 6600 | 6 | 340 |
| 5 | 7700 | 8 | 280 |
| 6 | 7700 | 6 | 280 |
| 7 | 6600 | 8 | 280 |
| 8 | 6600 | 6 | 280 |
| 9 | 9300 | 8 | 340 |
| 10 | 9300 | 6 | 340 |
| 11 | 9300 | 8 | 280 |
| 12 | 9300 | 6 | 280 |
| 13 | 7700 | 4 | 280 |
| 14 | 7700 | 4 | 340 |
| 15 | 9300 | 4 | 280 |
| 16 | 9300 | 4 | 340 |
| 17 | 6600 | 4 | 280 |
| 18 | 6600 | 4 | 340 |

**Table A2 - Full factorial design for two-armed MEMS switch**

| Design | Area (A) (um^2) | Arm width (b) (um) | Arm length (L) (um) | Meanders (M) (#) |
|---|---|---|---|---|
| 1 | 21200 | 5 | 300 | 4 |
| 2 | 21200 | 7 | 300 | 4 |
| 3 | 22600 | 5 | 300 | 4 |
| 4 | 22600 | 7 | 300 | 4 |
| 5 | 21200 | 5 | 320 | 4 |
| 6 | 21200 | 7 | 320 | 4 |
| 7 | 22600 | 5 | 320 | 4 |
| 8 | 22600 | 7 | 320 | 4 |
| 9 | 21200 | 5 | 300 | 3 |
| 10 | 21200 | 7 | 300 | 3 |
| 11 | 22600 | 5 | 300 | 3 |
| 12 | 22600 | 7 | 300 | 3 |
| 13 | 21200 | 5 | 320 | 3 |
| 14 | 21200 | 7 | 320 | 3 |
| 15 | 22600 | 5 | 320 | 3 |
| 16 | 22600 | 7 | 320 | 3 |

**Table A3 - Full factorial design for four-armed MEMS switch**